

SnTe doping of GaAs grown by atomic layer molecular beam epitaxy

M. Kuball, M. Cardona, A. Mazuelas, K. H. Ploog, J. J. PérezCamacho et al.

Citation: *J. Appl. Phys.* **77**, 4339 (1995); doi: 10.1063/1.359458

View online: <http://dx.doi.org/10.1063/1.359458>

View Table of Contents: <http://jap.aip.org/resource/1/JAPIAU/v77/i9>

Published by the [American Institute of Physics](http://www.aip.org).

Related Articles

The effects of group-I elements co-doping with Mn in ZnO dilute magnetic semiconductor
J. Appl. Phys. **111**, 123524 (2012)

Acceptor-like deep level defects in ion-implanted ZnO
Appl. Phys. Lett. **100**, 212106 (2012)

Characteristics of indium incorporation in InGaN/GaN multiple quantum wells grown on a-plane and c-plane GaN
Appl. Phys. Lett. **100**, 212103 (2012)

Effect of Li-doping on the magnetic properties of ZnO with Zn vacancies
J. Appl. Phys. **111**, 093902 (2012)

A new type of low temperature conductivity in InSb doped with Mn
AIP Advances **2**, 022116 (2012)

Additional information on *J. Appl. Phys.*

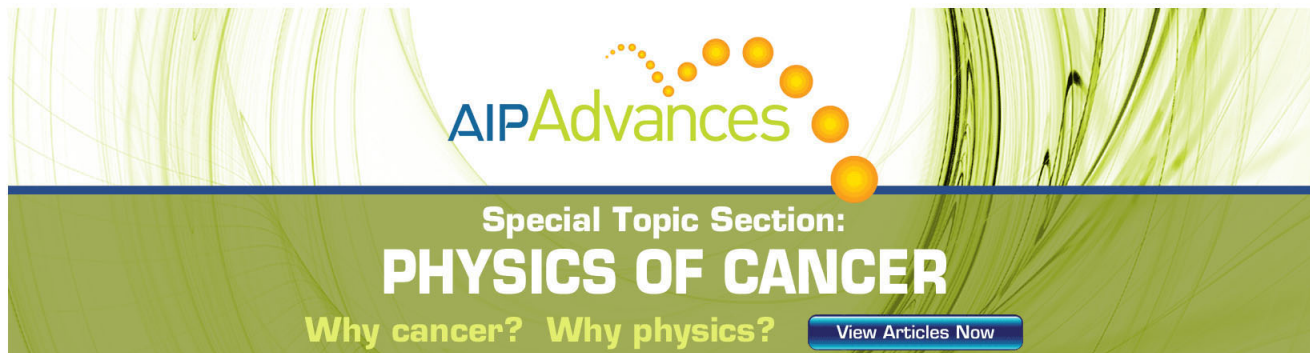
Journal Homepage: <http://jap.aip.org/>

Journal Information: http://jap.aip.org/about/about_the_journal

Top downloads: http://jap.aip.org/features/most_downloaded

Information for Authors: <http://jap.aip.org/authors>

ADVERTISEMENT



AIP Advances

Special Topic Section:
PHYSICS OF CANCER

Why cancer? Why physics? [View Articles Now](#)

SnTe-doping of GaAs grown by atomic layer molecular beam epitaxy

M. Kuball^{a)} and M. Cardona

Max-Planck-Institut für Festkörperforschung, Heisenbergstrasse 1, D-70569 Stuttgart, Germany

A. Mazuelas and K. H. Ploog

Paul-Drude-Institut für Festkörperelektronik, Hausvogteiplatz 5-7, D-10117 Berlin, Germany

J. J. Pérez-Camacho, J. P. Silveira, and F. Briones

Centro Nacional de Microelectrónica, Serrano 144, E-28006 Madrid, Spain

(Received 5 October 1994; accepted for publication 17 January 1995)

Using x-ray diffraction and ellipsometry we have studied the incorporation process of SnTe in GaAs for n-type doping. Combining these two techniques allows us to decide whether SnTe is incorporated pairwise, as has been proposed in the literature. We found SnTe doping to change the E_1 and $E_1 + \Delta_1$ critical point parameters in a way similar to that previously reported for n-type Si-doped GaAs. X-ray diffraction and Hall measurements show that the free carrier concentration is more than 1/2 of the $[\text{Sn}] + [\text{Te}]$ concentration. We thus conclude that a large proportion of SnTe is incorporated as independent Sn and Te dopant atoms. © 1995 American Institute of Physics.

I. INTRODUCTION

Molecular beam epitaxy (MBE) has evolved into one of the most important techniques for the fabrication of high quality semiconductor devices. Sn and Si are most widely used for n-type doping of GaAs in MBE. However, using Sn, sharp doping profiles are difficult to achieve due to the accumulation of Sn on the surface during growth.¹ This disadvantage may be overcome with the use of either Si or SnTe as a dopant.²⁻⁴ Sharp doping profiles were achieved using SnTe,^{4,5} however, the incorporation process of SnTe is still an open question. Collins *et al.*⁵ proposed SnTe to be incorporated pairwise, with its dissociation occurring only for growth temperatures above 580 °C. Calculations for paired donor impurities have been performed. They suggest that the SnTe pair levels are resonant with the conduction band.^{6,7}

It is well known that doping changes the optical response.⁸ The dependence on doping of the E_1 and $E_1 + \Delta_1$ critical points, which are responsible for two of the strongest features in the dielectric function, has been studied extensively.⁹⁻¹¹ These critical points originate from transitions in the Λ -direction of the Brillouin zone, i.e., for \mathbf{k} along $\langle 111 \rangle$.¹² Doping induces a critical point shift to lower energies and a broadening, which scale quadratically with dopant charge but show at most a linear dependence (usually weaker) on the dopant concentration.¹¹ Therefore, the study of the optical response should allow us to distinguish between mono- $[\text{Sn}^+ + \text{Te}^+, (\text{SnTe})^+]$ and divalent $[(\text{SnTe})^{2+}]$ donor atoms. However, ellipsometry cannot distinguish between $\text{Sn}^+ + \text{Te}^+$, and $(\text{SnTe})^+$. This problem can be overcome using x-ray diffraction to determine the impurity concentration $[\text{Sn}] + [\text{Te}]$.

In this article we present x-ray diffraction and ellipsometry (in the 1.7–5.7 eV range) measurements on n-type SnTe-doped GaAs(100) films (up to carrier concentrations of $1.2 \times 10^{19} \text{ cm}^{-3}$) at room temperature. The observed doping effect on the optical properties is found to be similar to that

recently reported for n-type Si-doped GaAs.¹¹ Combining with the results from x-ray diffraction, we conclude that a large proportion of SnTe is incorporated as independent Sn and Te donor atoms.

II. EXPERIMENT

A. Samples

A set of SnTe-doped n-type GaAs films of 5000 Å thickness (up to carrier concentrations of $1.2 \times 10^{19} \text{ cm}^{-3}$) was grown by atomic layer molecular beam epitaxy (ALMBE)² on semiinsulating GaAs(100) at a substrate temperature of $T_S = 350$ °C. During ALMBE growth the surface stoichiometry is periodically modulated between As-rich and Ga-stabilized reconstructions by periodically supplying As_4 beam pulses (0.4 s long, beam equivalent pressure of 3×10^{-6} mb), while Ga flux is continually supplied to provide a rate of 0.8 monolayers/s ($\sim 0.8 \mu\text{m/h}$) as in conventional MBE. The growth kinetics obtained by this modulation induces a layer by layer deposition and allows to reduce substrate temperatures from the standard 580–600 °C to 300–350 °C, in order to improve dopant incorporation without compromising the optical quality. Surface morphology is also excellent (mirrorlike under Nomarski microscope), even for the highest doping levels. The dopant concentration was changed by varying the SnTe cell temperature between $T_S = 300$ and 369 °C. Further details about the sample growth will be published elsewhere.¹³ The free carrier concentration was determined by Hall measurements at room temperature.

B. X-ray diffraction

X-ray diffraction measurements were performed using a double crystal diffractometer with a Cu anode $[\lambda(\text{Cu}_{K\alpha 1}) = 1.54056 \text{ \AA}]$ and a (100) asymmetrically cut Ge crystal as monochromator and collimator. Dynamical simulations of the diffraction patterns were performed in order to determine the perpendicular strain (ϵ_{zz}), the $[\text{Sn}] + [\text{Te}]$ con-

^{a)}Electronic mail: kuball@cardix.mpi-stuttgart.mpg.de

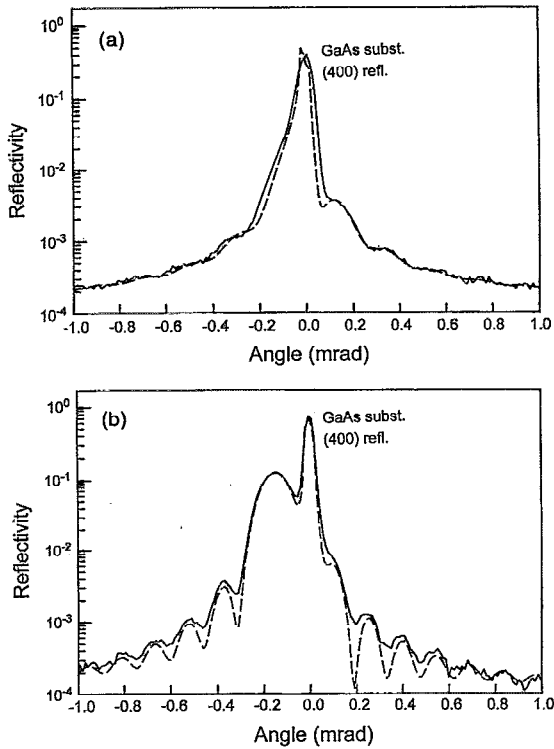


FIG. 1. X-ray diffraction pattern of (a) the $n=3.0 \times 10^{18} \text{ cm}^{-3}$ (No. 1) and (b) the $n=1.16 \times 10^{19} \text{ cm}^{-3}$ -doped GaAs sample (No. 8) (full lines). The dashed lines represent fitted line shapes.

centration and to assess the structural quality of the layers. We follow the scheme proposed by Tapfer *et al.*¹⁴

C. Ellipsometry

The complex dielectric function of the variously SnTe-doped GaAs samples was determined using rotating analyzer ellipsometry. A detailed description of this technique can be found elsewhere in the literature.¹⁵ The samples were measured without any chemical treatment of the surface (i.e., as grown). The complex dielectric function was evaluated from the measured ellipsometric angles using a three-phase model (ambient-oxide-bulk). Since the penetration depth of light is much smaller than the film thickness throughout the entire spectral range investigated, we have neglected the finite film thickness in this analysis. The oxide layer thickness was assumed to be the same for all samples and was determined by fitting the ellipsometric data of an undoped GaAs sample in the region of the E_2 gap using the dielectric functions of undoped GaAs and its oxide, as found in the literature.^{16,17} The E_1 and $E_1 + \Delta_1$ critical points were treated as two-dimensional critical points having the canonical line shape¹²

$$\epsilon(\omega) \propto C - \ln(\hbar\omega - E + i\Gamma) e^{i\Phi}, \quad (1)$$

where E represents the critical point energy, Γ the broadening and Φ the phase angle. The critical point parameters were determined by fitting the numerically obtained second derivative spectrum $\partial^2 \epsilon / \partial E^2$.

TABLE I. Fitting parameters of the XRD patterns: $\epsilon_{zz} = (a_{\perp} - a_0)/a_0$ denotes the perpendicular strain and $[\text{Sn}]+[\text{Te}]$ the impurity concentration. The relative error of $[\text{Sn}]+[\text{Te}]$ is the same as the one of ϵ_{zz} . n is the free carrier concentration as determined from Hall measurements at room temperature.

Sample No.	n (10^{19} cm^{-3})	ϵ_{zz} (10^{-4})	$\Delta \epsilon_{zz} / \epsilon_{zz}$ (10^{-2})	$[\text{Sn}]+[\text{Te}]$ (10^{19} cm^{-3})	$\alpha = n / ([\text{Sn}]+[\text{Te}])$
1	0.30	0.45	25	0.4(0)	0.75
2	0.40	0.50	20	0.4(2)	0.95
3	0.54	0.90	10	0.7(9)	0.68
4	0.58	1.10	9	0.9(1)	0.64
5	0.84	1.90	2.5	1.5(8)	0.53
6	0.90	1.70	3	1.4(1)	0.64
7	1.08	2.33	1	1.9(3)	0.56
8	1.16	2.62	1	2.1(7)	0.53

III. RESULTS

A. X-ray diffraction

Figure 1 illustrates the effect of doping on the x-ray diffraction (XRD) pattern (full lines). Dynamical simulations of the diffraction patterns were performed following the scheme proposed by Tapfer *et al.*¹⁴ to determine the perpendicular strain $\epsilon_{zz} = (a_{\perp} - a_0)/a_0$ and therefrom the impurity concentration $[\text{Sn}]+[\text{Te}]$. The results of the line shape fitting (dashed lines in Fig. 1) are given in Table I. The maximum value of the perpendicular strain ϵ_{zz} is 2.62×10^{-4} , small enough not to produce any relaxation of the layers. The ratio $\alpha = n / ([\text{Sn}]+[\text{Te}])$ of the free carrier concentration n to the impurity concentration $[\text{Sn}]+[\text{Te}]$ decreases as the doping increases, i.e., from about 0.75–0.95 at $[\text{Sn}]+[\text{Te}] = 0.4 \times 10^{19} \text{ cm}^{-3}$ to 0.53 at $[\text{Sn}]+[\text{Te}] = 2.1 \times 10^{19} \text{ cm}^{-3}$ as illustrated in Fig. 2. Different incorporation processes of SnTe in GaAs appear to be possible:

- (i) $\text{Sn}^+, \text{Te}^+ \quad \alpha = 1.0$
- (ii) $(\text{SnTe})^+ \quad \alpha = 0.5$
- (iii) $(\text{SnTe})^{2+} \quad \alpha = 1.0.$

The incorporation of electrically inactive Sn or Te atoms as reported by Collins *et al.*⁵ and the appearance of DX centers

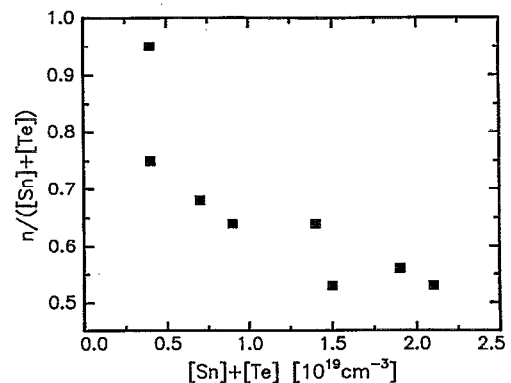


FIG. 2. Ratio $\alpha = n / ([\text{Sn}]+[\text{Te}])$ of the free carrier concentration n to the impurity concentration $[\text{Sn}]+[\text{Te}]$ vs the impurity concentration $[\text{Sn}]+[\text{Te}]$.

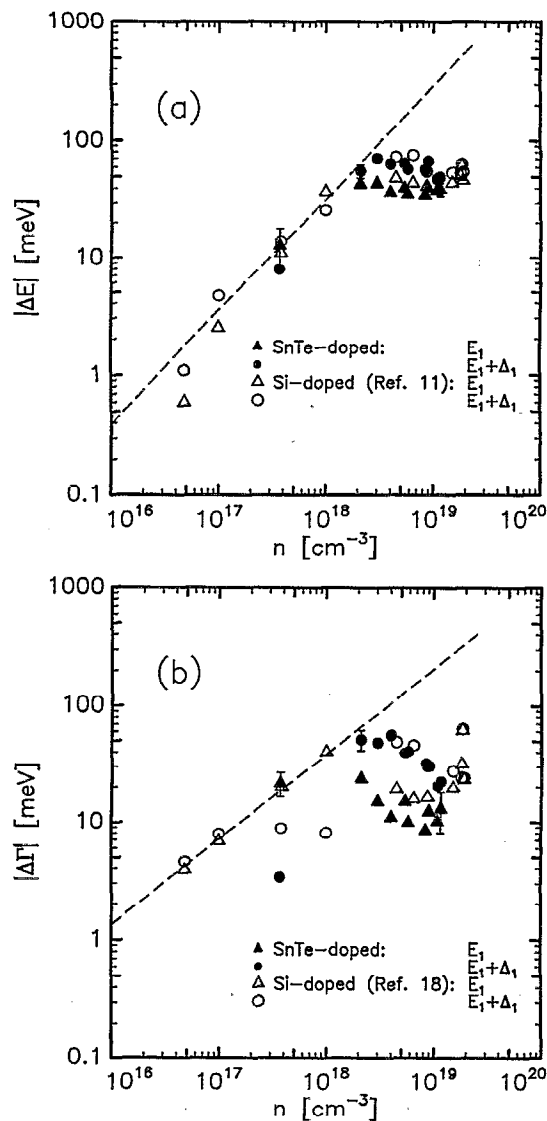


FIG. 3. Dependence of (a) the E_1 and $E_1 + \Delta_1$ critical point energies $|\Delta E| = |E_{\text{doped}} - E_{\text{undoped}}|$ and (b) broadenings $|\Delta \Gamma| = |\Gamma_{\text{doped}} - \Gamma_{\text{undoped}}|$ on the carrier concentration n for n-type SnTe-doped GaAs, as well for n-type Si-doped GaAs (from Refs. 11 and 18).

or other deep defects should explain the decrease in α with doping at high doping levels. Similar effects were observed in Si-doped GaAs.¹⁹ The inclusion of Sn as an acceptor would be another possible mechanism for the reduction of α at high doping levels, however, should play a minor role.^{20–22} We thus conclude that, at least for low doping levels, SnTe is mainly incorporated either as Sn^+ and Te^+ or as $(\text{SnTe})^{2+}$.

B. Ellipsometry

Doping induces a red shift ($|\Delta E| = |E_{\text{doped}} - E_{\text{undoped}}|$) and broadening ($|\Delta \Gamma| = |\Gamma_{\text{doped}} - \Gamma_{\text{undoped}}|$) of the E_1 and $E_1 + \Delta_1$ critical points in n-type SnTe-doped GaAs. Their dependence on the carrier concentration is shown in Fig. 3 in a log-log representation. SnTe doping shows, within our ex-

perimental resolution, identical results to those previously observed on Si-doped GaAs,^{11,18} which are reproduced in Fig. 3. The red shift and broadening follows a power-law dependence n^α ($\alpha_E = 0.96 \pm 0.10$, $\alpha_\Gamma = 0.75 \pm 0.10$)^{11,18} on the carrier concentration n up to about $n = 3 \times 10^{18} \text{ cm}^{-3}$, whereas at higher doping levels a saturation (or even a slight decrease in the case of the broadening) is observed.

Doping results in a change of the bulk optical properties due to the influence of the dopant potentials which are screened by the free carriers:⁹ a red shift and broadening of the E_1 and $E_1 + \Delta_1$ critical points result. However, band bending effects present on most surfaces due to surface Fermi level pinning,²³ conceal the bulk behavior. Only cleaved GaAs(110), having flat bands at the surface due to the absence of surface states within the gap,²³ allows the study of the bulk doping effect.¹¹ In all other cases, the removal of the free carriers from the surface depletion layer increases the dopant potential influence—the unscreening of impurities—and results, therefore, in a significantly larger red shift and broadening of the critical points as compared to bulk.¹¹ In fact, in the low doping regime, where the depletion layer thickness exceeds the penetration depth of light, only this region is probed. The effect of the unscreening of impurities can be estimated using second order perturbation theory omitting the \mathbf{k} dependence of the wave functions and applying simple screening theory with a screening, i.e., cut-off length, λ^{-1} proportional to the average distance between impurities:^{10,11}

$$\Delta E_{\mathbf{k},l} \approx N \sum_{\mathbf{q},m} \left[\frac{4\pi \cdot (Ze) \cdot e}{q^2 + \lambda^2} \right]^2 \frac{1}{E_{\mathbf{k},l} - E_{\mathbf{k}+\mathbf{q},m}},$$

$$\lambda^{-1} \propto N^{-1/3}, \quad (2)$$

where N denotes the dopant concentration and Z the dopant charge. The redshift of the critical point energy follows the law $\Delta E \propto N^{-1/3}$ for small, and $\Delta E \propto N$ for large \mathbf{q} vector contributions. The linear increase observed in the experiment in the low-doping regime [Fig. 3(a)] point to dominant large \mathbf{q} vector contributions. Note that since the electric field in the depletion layer has been shown to play only a minor role,¹¹ we have neglected its effect.

At the carrier concentration n , divalent donors ($N = n/2, Z = 2$), e.g., $(\text{SnTe})^{2+}$, result, therefore, in twice as large a doping effect as monovalent donors ($N = n, Z = 1$), e.g., $\text{Sn}^+ + \text{Te}^+$ or $(\text{SnTe})^+$. Note that $(\text{SnTe})^{2+}$ represents to a first approximation a divalent donor. Since SnTe doping gives the same doping effect as Si doping, monovalent donors play the dominant role in SnTe-doped GaAs. However, ellipsometry can not distinguish between $\text{Sn}^+ + \text{Te}^+$ and $(\text{SnTe})^+$. $(\text{SnTe})^+$ pairs would result in $\alpha = n / ([\text{Sn}] + [\text{Te}]) = 0.5$. Electrically inactive Sn or Te, as well as DX centers or other deep defects appearing at higher dopings reduce α , so that the measured value for α would be smaller than 0.5.^{5,24} However, the ratio of n to $[\text{Sn}] + [\text{Te}]$ obtained experimentally by Hall and XRD shows that α is in the range of 0.95–0.53 (Table I, Fig. 2). Therefore it is obvious that, at least for low doping levels, ellipsometry and XRD conclude that Sn^+, Te^+ is the dominant doping mechanism. This is in contrast to the pairwise incorporation process

previously proposed in the literature for growth temperatures below 580 °C which is the case for our samples.⁵

Note that at high doping levels bulk doping behavior starts to contribute:^{10,11}

$$\Delta E \propto \frac{Z}{m_{\Gamma}^{*3/2}} n^{1/2}, \quad (3)$$

since the depletion layer width reduces below the light penetration depth. This results in a weakening of the doping dependence.¹¹ Again mono and divalent donor result in different changes allowing the same conclusion as above. The same conclusions can be drawn by considering the doping-induced broadening of the critical points [Fig. 3(b)].^{9,18}

DX centers, which are always present in these highly doped GaAs samples,²⁴ were not taken into account in the ellipsometry analysis since it has been pointed out that they do not significantly influence the critical point parameters.¹¹

IV. CONCLUSION

A series of n-type GaAs:SnTe layers were grown by ALMBE at low temperature ($T_S=350$ °C). The incorporation process of SnTe in GaAs was studied using x-ray diffraction and ellipsometry. Combining these two techniques we are able to distinguish between the doping mechanisms:

(i) Sn^+ , Te^+ ,

(ii) $(\text{SnTe})^+$,

(iii) $(\text{SnTe})^{2+}$.

The similar doping effect on the E_1 and $E_1 + \Delta_1$ critical points for SnTe doping as compared to Si doping rules out $(\text{SnTe})^{2+}$ pairs. The experimental $n/([\text{Sn}] + [\text{Te}])$ values obtained by Hall and XRD measurements show therefore Sn^+ , Te^+ to be the dominant doping mechanism, at least for low doping levels.

ACKNOWLEDGMENTS

We are indebted to F. Garcia for helpful discussions, P. Wurster, M. Siemers, and H. Hirt for technical assistance. A. M. and J. P. S. acknowledge the financial support of Ministerio de Educación y Ciencia of Spain.

- ¹ K. Ploog and A. Fischer, *J. Vac. Sci. Technol.* **15**, 225 (1978).
- ² F. Briones, L. González, and A. Ruiz, *Appl. Phys. A* **49**, 729 (1989).
- ³ J. P. Silveira and F. Briones, *Appl. Phys. Lett.* **65**, 573 (1994).
- ⁴ D. M. Collins, *Appl. Phys. Lett.* **35**, 67 (1979).
- ⁵ D. M. Collins, J. N. Miller, Y. G. Chai, and R. Chow, *J. Appl. Phys.* **53**, 3010 (1982).
- ⁶ O. F. Sankey and J. D. Dow, *Appl. Phys. Lett.* **38**, 685 (1981).
- ⁷ S.-F. Ren, K. E. Newman, J. D. Dow, and O. F. Sankey, *Appl. Phys. A* **33**, 269 (1984).
- ⁸ M. Cardona, K. L. Shaklee, and F. H. Pollak, *Phys. Rev. B* **154**, 696 (1967).
- ⁹ L. Viña and M. Cardona, *Phys. Rev. B* **29**, 6739 (1984).
- ¹⁰ F. Lukšs, S. Gopalan, and M. Cardona, *Phys. Rev. B* **47**, 7071 (1993).
- ¹¹ M. Kuball, M. K. Kelly, K. Köhler, and J. Wagner, *Phys. Rev. B* **49**, 16 569 (1994).
- ¹² P. Lautenschlager, M. Garriga, S. Logothetidis, and M. Cardona, *Phys. Rev. B* **36**, 4821 (1987).
- ¹³ J. J. Pérez-Camacho, J. P. Silveira, F. Garcia, F. Briones, A. Mazuelas, and K. H. Ploog (unpublished).
- ¹⁴ L. Tapfer and K. Ploog, *Phys. Rev. B* **40**, 9802 (1989); C. Giannini, A. Fischer, C. Lange, K. Ploog, and L. Tapfer, *Appl. Phys. Lett.* **61**, 183 (1992).
- ¹⁵ See, e.g., R. M. A. Azzam and N. M. Bashara, *Ellipsometry and Polarized Light* (North Holland, Amsterdam, 1977).
- ¹⁶ D. E. Aspnes and A. A. Studna, *Phys. Rev. B* **27**, 985 (1983).
- ¹⁷ D. E. Aspnes, G. P. Schwarz, G. J. Gualtieri, A. A. Studna, and B. Schwartz, *J. Electrochem. Soc.* **128**, 590 (1981).
- ¹⁸ M. Kuball, M. K. Kelly, P. V. Santos, M. Cardona, K. Köhler, and J. Wagner, to be published in *Proceedings of the 22th International Conference on the Physics of Semiconductors*, Vancouver, Canada, 1994.
- ¹⁹ M. Ramsteiner, J. Wagner, P. Hiesinger, K. Köhler, and U. Rössler, *J. Appl. Phys.* **73**, 5023 (1993).
- ²⁰ H. Ito and T. Ishibashi, *Jpn. J. Appl. Phys.* **26**, L1760 (1987).
- ²¹ K. F. Longenbach, S. Xin, and W. I. Wang, *J. Appl. Phys.* **69**, 3393 (1991).
- ²² M. Ramsteiner, J. Wagner, J. P. Silveira, and F. Briones, *Gallium Arsenide and Related Compounds 1990, Proceedings of the Seventeenth International Symposium*, Jersey, UK, edited by K. E. Singer (IOP, Bristol, 1990), pp. 85–90.
- ²³ H. Lüth, M. Büchel, R. Dorn, M. Liehr, and R. Matz, *Phys. Rev. B* **15**, 865 (1977).
- ²⁴ P. M. Mooney, *J. Appl. Phys.* **67**, R1 (1990), and references therein.